ASSESSMENT OF ACOUSTIC TRAVEL-TIME TOMOGRAPHY OF THE ATMOSPHERIC SURFACE LAYER

D. Keith Wilson,[*,1] Vladimir E. Ostashev,[2,3] Sergey N. Vecherin,[3]
Alexander G. Voronovich,[2] Sandra L. Collier,[4] John M. Noble[4]

[1]U.S. Army Cold Regions Research and Engineering Laboratory, Hanover, New Hampshire
[2]NOAA Environmental Technology Laboratory, Boulder, Colorado
[3]New Mexico State University, Las Cruces, New Mexico
[4]U.S. Army Research Laboratory, Adelphi, Maryland

1. INTRODUCTION

In-situ measurements from isolated vertical towers provide only a very limited picture of multi-dimensional flow structure in the atmosphere. For purposes such as examining the role of coherent structures in the near-ground atmosphere, characterizing flow patterns in complex terrain, and developing large-eddy simulation (LES) subgrid-scale models, observation techniques that extend beyond the limitations of single instrumented towers are necessary. Volume-imaging lidar and radar technologies have progressed rapidly in recent years, and these systems are now providing detailed, multi-dimensional images of the atmospheric boundary layer (ABL). There still appears to be a need, however, for an inexpensive, multi-dimensional observation system for near-ground flow imaging on the scale of tens to hundreds of meters. Such observations have usually been supplied previously by dense arrays of vertical towers. An alternative technique, which is still in a developmental stage, is acoustic tomography (Wilson et al., 2001).

Acoustic tomography uses the travel times of pulses (which depend on wind velocity and temperature) to reconstruct regions of the medium through which they propagate. Travel-time tomography is being used today, with much success, to image the ocean and solid Earth. The feasibility of acoustic tomography of the near-ground atmosphere has been previously demonstrated in several field studies, e.g., Wilson and Thomson (1994) and Ziemann et al. (1999). However, a quantitative examination of the accuracy of the methodology is difficult, because the tomographic observations are averages along lines (the propagation paths between the sources and receivers) and therefore cannot be directly compared to point observations in the atmosphere. The value of tomography in comparison to observations from multiple, in-situ vertical towers also needs to be examined more critically.

We begin this paper with a general discussion of the problem of "inverting" a finite set of line or point measurements to reconstruct a continuous turbulence field. Statistical methods are used to study errors resulting from imperfect and incomplete information used during the inversion process. We then assess the performance of acoustic tomography numerically by simulating both the direct and inverse problems. Realistic, high-resolution turbulence fields are synthesized in the tomographic plane using the quasi-wavelet method. Sound is propagated through these fields to obtain travel-time data. Various inverse methods, based on grid-cell partitioning of the tomographic plane as well as on continuous field reconstructions, are then applied and the accuracy in imaging the original turbulence field is ascertained.

2. INVERSION OF TOMOGRAPHIC AND POINT DATA

Consider the general problem of reconstructing atmospheric fields from a set of indirect observations. The observations d_i, where $i = 1, \ldots, N_d$, are arranged as a column vector $\mathbf{d}$. In the normal parlance of inverse problems, $\mathbf{d}$ is called the *data* vector. Similarly, suppose a number of samples of the atmospheric fields, m_j, where $j = 1, \ldots, N_m$, are arranged as a column vector $\mathbf{m}$. These atmospheric fields may sample different points in space and/or multiple fields.[1] The quantity $\mathbf{m}$ is referred to as the *model* vector. The general, linear inverse problem is to construct an operator $\mathbf{G}_x^{-1}$ that allows a good estimate $\hat{\mathbf{m}}$ of the actual $\mathbf{m}$ to be determined from $\mathbf{d}$:

$$\hat{\mathbf{m}} = \mathbf{G}_x^{-1}\mathbf{d}. \qquad (1)$$

It can be shown that the optimal inverse operator, in the sense of minimizing the expected mean-square errors $\langle e_j^2 \rangle = \left\langle (\hat{m}_j - m_j)^2 \right\rangle$ (where the angle brackets indicate the statistical expectation), is

$$\mathbf{G}_s^{-1} = \mathbf{R}_{md}\mathbf{R}_{dd}^{-1}, \qquad (2)$$

in which $\mathbf{R}_{md} = \left\langle \mathbf{m}\widetilde{\mathbf{d}} \right\rangle$ is the model-data covariance matrix and $\mathbf{R}_{dd} = \left\langle \mathbf{d}\widetilde{\mathbf{d}} \right\rangle$ is the data-data covariance matrix.

Corresponding author address: D. Keith Wilson, U.S. Army Cold Regions Research and Engineering Laboratory, 72 Lyme Rd., Hanover, NH 03755-1290; e-mail: D.Keith.Wilson@erdc.usace.army.mil.

[1]The models and data are usually taken to be perturbations about a reference state. Conceptually, the models may be any atmospheric field(s). In this paper, they are the sound speed (which depends primarily on temperature) and wind velocity components. The data may consist of point observations of the sound speed or wind velocity, or, for the tomograpy, the travel-time of a signal along a trajectory connecting a source/receiver pair.

(The tilde indicates matrix transposition.) The operator $\mathbf{G}_s^{-1}$ is called the *stochastic inverse* by Aki and Richards (1980).

To complete the formulation, we need a statistical model for the covariance matrices. Typically, the data $\mathbf{d}$ are assumed to depend linearly on the underlying atmospheric fields. One can then calculate $\mathbf{R}_{md}$ and $\mathbf{R}_{dd}$ from knowledge of the spatial correlation functions of the atmospheric fields. If $\mathbf{d}$ consists of point observations of atmospheric fields, this process is trivial. For example, suppose $\mathbf{d}$ is a set of in-situ temperature measurements at an array of towers, and we wish to construct the model $\mathbf{m}$ at intermediate points. Then $\mathbf{R}_{md}$ is simply the correlation function for the temperature field between the observation points and the points of the reconstruction, and $\mathbf{R}_{dd}$ consists of the correlations between the temperatures at the observation points. The situation for tomography is a bit more complicated: one must relate the travel-time of the acoustic pulses to the atmospheric fields along their trajectories. But, this is a well defined problem and its solution is discussed, for example, in Wilson and Thomson (1994).

The principle difficulty in setting up the optimal stochastic inverse is that the correlation functions for the atmospheric fields are not known in advance. It is possible to estimate $\mathbf{R}_{dd}$ from an observational dataset, since a time series of the data are available. The same cannot be said of $\mathbf{R}_{md}$, because there is no access to the atmospheric fields at the reconstruction points. Therefore, the optimal (*true*) stochastic inverse is actually unattainable in most real-world problems. The best we can hope for is a reasonable approximation to the optimal inverse.

Given that the correlation function of the atmospheric fields is unknown, it may initially seem desirable to adopt alternative approaches to the inverse problem that are "agnostic" with regard to the structure of the atmospheric fields to be reconstructed (the model space). But, in actuality, inverse methods that initially appear agnostic often make very significant assumptions about the atmospheric correlation function. For example, an inverse technique that partitions the atmosphere into a finite number of grid cells in effect assumes that the fields are perfectly correlated between two points within each cell, and are completely uncorrelated between points in different grid cells. This step behavior for the correlation function is unrealistic in a fluid medium, as it forces a discontinuous solution on a continuous field.

Reconstruction of atmospheric fields based on interpolations between observation points also makes implicit assmptions about the spatial correlation functions. The correlations depend on the spline of the particular interpolation method. For example, if linear interpolation is used, the underlying correlation functions would consist of a sequence of linear regions. It is also common to reconstruct the atmospheric fields from a discrete set of measurements by fitting the measurements with a truncated harmonic series. Such a procedure, by setting the high wavenumber components of the medium to zero, implies a correlation function that is artificially high for small spatial separations.

This reasoning should not be construed as implying that inverse methods based on gridding of the atmospheric fields, interpolation, or truncated harmonic series are inherently poor. In application, these approaches may lead to satisfactory inverse solutions while offering benefits such as low computational effort. The point to be made is that they are not agnostic as far as the correlation structure of the atmospheric fields. The underlying assumptions may just not be as obviously evident. Since the problem of reconstructing a continuous medium from finite measurements is inherently an underdetermined one, it would seem impossible to devise inverse methods that do not involve assumptions about the spatial structure of the model space.

Since the true stochastic inverse cannot be calculated in practice, the question arises whether the stochastic inverse formalism provides good results when a correlation function somewhat different from that of the actual atmosphere is used. One could view the correlation function used to calculate the stochastic inverse as a sort of smoothing function. For example, data are collected at observation points spaced at an average distance L, a Gaussian correlation function with length scale set to L might be used to calculate the stochastic inverse. The reconstructed atmospheric fields would then be reconstructed with smoothing at a scale corresponding to the spacing between the observation points. When viewed in this regard, the stochastic inverse is quite similar to smooth interpolation between the observation points. The discussion is complicated somewhat when the observations consist of line averages (such as in a tomography experiment), but the basic idea remains of viewing the correlation function in the stochastic inverse as the basis for smoothing the reconstruction.

3. ERROR MAPS AND CORRELATION FUNCTIONS

To assess the accuracy of a particular inverse operator $\mathbf{G}_x^{-1}$, the error-error covariance matrix (defined as $\mathbf{R}_{ee} = \langle \mathbf{e}\widetilde{\mathbf{e}} \rangle$, where $\mathbf{e} = \widehat{\mathbf{m}} - \mathbf{m}$) may be calculated. It can be shown that

$$\mathbf{R}_{ee} = \mathbf{R}_{mm} - \mathbf{G}_x^{-1}\widetilde{\mathbf{R}}_{md} - \mathbf{R}_{md}\widetilde{\mathbf{G}}_x^{-1} + \mathbf{G}_x^{-1}\mathbf{R}_{dd}\widetilde{\mathbf{G}}_x^{-1}, \quad (3)$$

where $\mathbf{R}_{mm}$ is the model-model covariance. Although knowledge of the correlation function of the atmospheric fields is not necessarily required to calculate a particular inverse operator $\mathbf{G}_x^{-1}$, the correlation function is required to calculate $\mathbf{R}_{mm}$, $\mathbf{R}_{md}$, and $\mathbf{R}_{dd}$ in (3) and thereby assess the error associated with the inverse operator.

For the optimal stochastic inverse, (3) simplifies to

$$\mathbf{R}_{ee} = \mathbf{R}_{mm} - \mathbf{R}_{md}\mathbf{R}_{dd}^{-1}\widetilde{\mathbf{R}}_{md}. \quad (4)$$

Since the second term on the right of (4) is positive definite, the stochastic inverse always reduces the diagonal elements of $\mathbf{R}_{mm}$ (the *a priori* variance of the atmospheric fields). The resulting diagonal elements of $\mathbf{R}_{ee}$ are the theoretical lower bound on the error of the reconstructed fields.
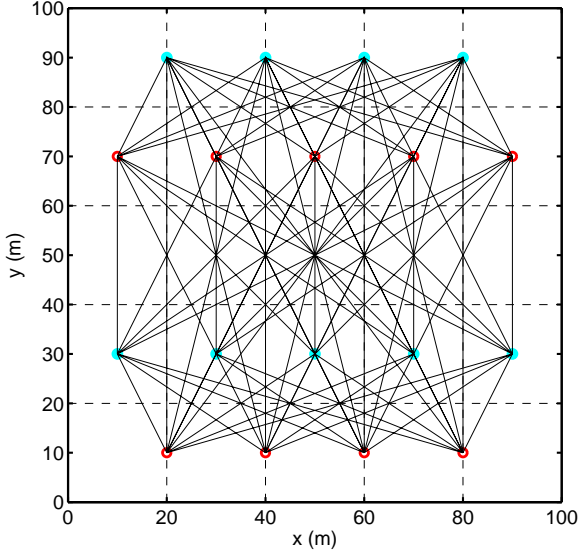
FIG. 1: Sensor array used for example calculations in this paper. The region is a horizontal one with dimensions 100 m × 100 m. Open, red circles indicate source locations and closed, cyan circles indicate receiver locations for the tomography. For point measurements, sensors are placed at each source and receiver location. Solid lines indicate ray paths for tomographic inversions. Dashed lines indicate boundaries of grid cells used for construction of the generalized inverse.

We now consider some example error calculations that demonstrate the effect of a mismatch between the presumed and actual correlation functions for the medium. The sensor array used for all calculations is shown in Figure 1. The figure shows the locations of acoustic sources (open circles) and receivers (closed circles), and all propagation paths connecting them. For comparisons involving point sensors, the sensors were placed at the same locations as the sources and receivers. There are a total of 9 sources and 9 receivers, which results in 81 propagation paths. In comparison, there are only 18 point sensors.[2]

For simplicity, our initial examples are based on an unknown scalar (e.g., a temperature or sound-speed perturbation). The actual correlation function for the medium is postulated to correspond von Kármán's spectrum, specifically

$$ f(r) = \frac{2\sigma^2}{\Gamma(1/3)} \left(\frac{r}{2\ell_K} \right)^{1/3} K_{1/3} \left(\frac{r}{\ell_K} \right), \qquad (5) $$

where r is the distance between two points, σ^2 is the variance of the field, and ℓ_K is the outer length-scale

---

[2]The configurations considered here are 2D planar arrays. The same inverse techniques can also be applied to 3D arrays. Alternatively, one could build a 2D, vertical planar array, perpendicular to the mean wind, and then use Taylor's frozen turbulence hypothesis to determine structure parallel to the wind.
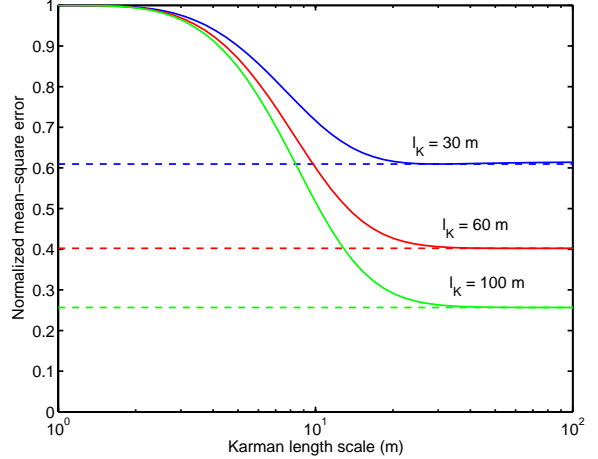

FIG. 2: Errors produced by the von Kármán correlation function model for various mismatches between the actual and presumed length scales. The mean-square error for the field point $(x, y) = (30\,\text{m}, 40\,\text{m})$ is shown. Solid lines are the minimum error attainable (when the actual and presumed length scales match) for actual length scales ℓ_K = 30, 60, and 100 m. Dashed lines vary the presumed correlation length scale.
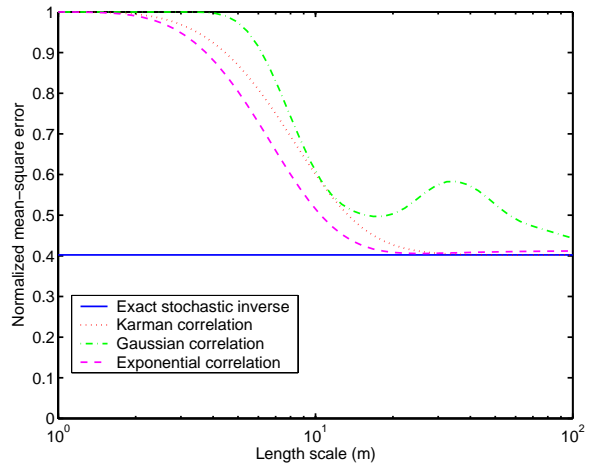

FIG. 3: Comparison of errors from von Kármán, Gaussian, and exponential correlation function models. The mean-square error for the field point (30 m, 40 m) is shown. Solid line is the minimum error attainable (when the actual and presumed length scales match). Dashed lines show the effect of varying the length scales used in the different correlation models.

parameter for the von Kármán model. (The term "outer length scale" is used here to indicate a length scale near the boundary between the energy-containing and inertial subranges. It is approximately equal to the integral length scale.) Other correlation functions we consider are the
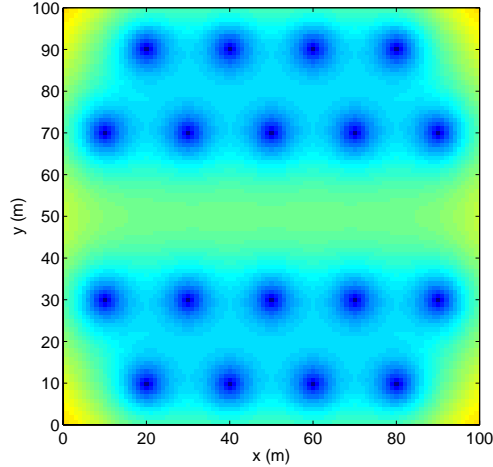
FIG. 4: Map of the mean-square error associated with reconstruction of a scalar field from measurements at 18 point sensors. The turbulence has a von Kármán correlation function with length scale ℓ_K = 60 m. The same correlation function is used in the field reconstruction.

FIG. 5: Same as Figure 4, except that the correlation function used in the field reconstruction is Gaussian with ℓ_G = 60 m.

Gaussian

$$f(r) = \sigma^2 \exp\left(-\frac{r^2}{\ell_G^2}\right), \tag{6}$$

and exponential

$$f(r) = \sigma^2 \exp\left(-\frac{r}{\ell_e}\right). \tag{7}$$

Note that ℓ_K, ℓ_G, and ℓ_e are defined differently and therefore are not presumed equal.

Figure 2 shows the effect of mismatches in the von Kármán length scale on the error at an example model reconstruction point, (x, y) = (30 m, 40 m). These calculations are for the point-sensor experiment. Three "actual" values of the length scale are considered: ℓ_K = 30, 60, and 100 m. The dashed lines indicate the lower bound on the error, as determined from (4). The solid lines show the error when the stochastic inverse is reconstructed with a value ranging from ℓ_K = 1 to 100 m. When the presumed value of ℓ_K is close to or larger than the actual value, the error is essentially at the lower limit. A significant increase in the error only occurs when too small a value for ℓ_K is used. The nearest sensor to the model point is 10 m distant. If the value of ℓ_K is smaller than 10 m, the stochastic inverse determines that the data provide little information at the model point. Therefore, the perturbation in the reconstructed field at the model point is set close to zero. In actuality, because the correlation between the available data and the model are rather high for all considered actual values of ℓ_K, the presumed lack of information was incorrect and led to an unnecessarily high error.

Figure 3 is similar to 2, except that the effect of assuming an incorrect shape to the correlation function is shown. The actual spectrum is assumed to be von Kármán's, with ℓ_K = 60 m, and the error at the model recon-
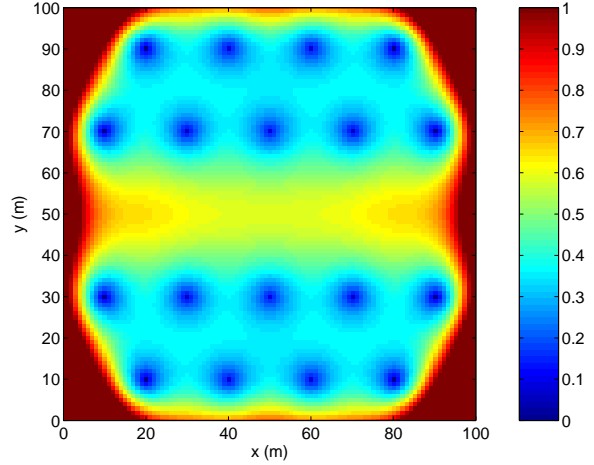

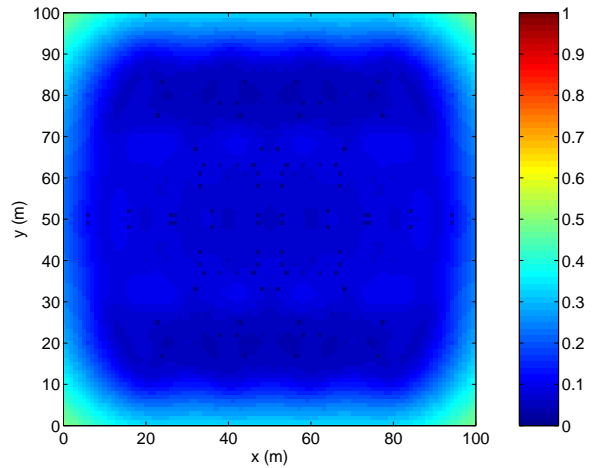FIG. 6: Same as Figure 4, except that the mean-square error is shown for a tomography experiment with 81 ray paths.

struction point (x, y) = (30 m, 40 m) is again shown. Interestingly, the exponential correlation function performs very similarly to the von Kármán correlation. For sufficiently large length scales, either choice provides nearly optimal reconstructions. The Gaussian correlation function, however, produces comparatively larger errors, particularly when $\ell_G \simeq 35$ m. This is likely related to the behavior of the second derivative for the Gaussian correlation function: it changes sign from negative to positive at $r = \ell_G/\sqrt{2}$, whereas the von Kármán and exponential correlations have positive second derivatives for all r.

Figures 4–6 show 2-D error map images (diagonal elements of $\mathbf{R}_{ee}$) for various inverses. In each example, the actual spectrum for the turbulence is von Kármán's, with ℓ_K = 60 m. The first example, Figure 4, is for point
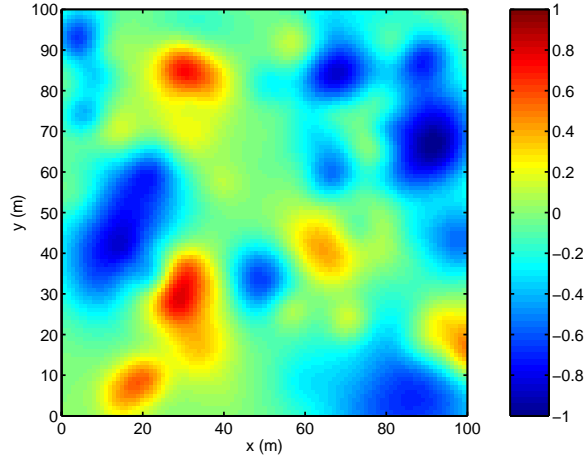
FIG. 7: Turbulent sound-speed field randomly synthesized by the QW method. Color scale is the speed in $m\,s^{-1}$.
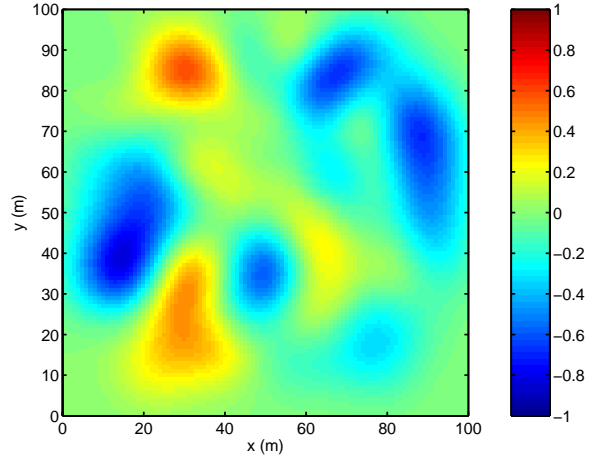

FIG. 9: Tomographic reconstruction of the sound speed based on ray paths through the fields shown in Figure 7 using the stochastic inverse method.
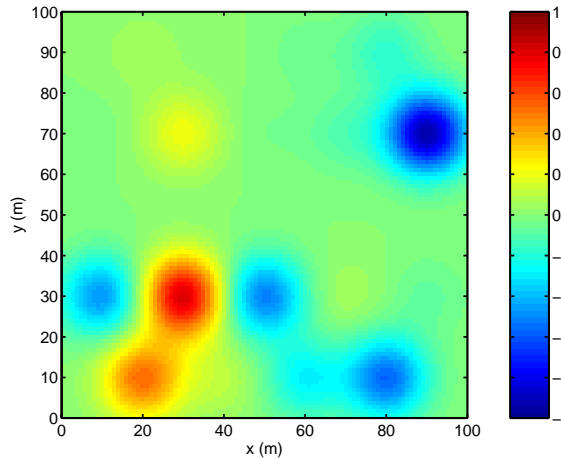

FIG. 8: Point-measurement reconstruction of the sound speed based on observations of the fields shown in Figure 7.
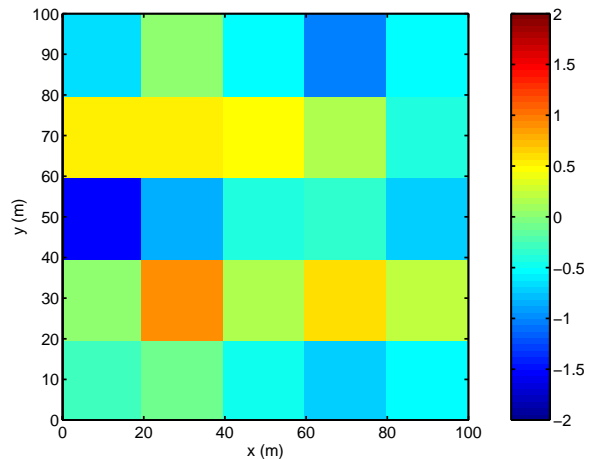

FIG. 10: Tomographic reconstruction of the sound speed based on ray paths through the fields shown in Figure 7 using the generalized inverse method.

4. SCALAR FIELD RECONSTRUCTIONS

sensors at the locations indicated in Figure 1. The presumed spectrum matches the actual one, so that the error map is the optimal stochastic inverse. As would be expected, the error is zero at the point sensor locations and increases gradually away from the sensors. Figure 5 is the same as 4, except that the presumed spectrum is Gaussian with $\ell_G = 60$ m. In this case, the error increases rather dramatically outside the areas with dense sensors. Figure 6 shows the optimal stochastic inverse for sources and receivers positioned as in Figure 1. The increase in the number of data (from 18 to 81) and path averaging has led to a dramatic improvement in the information available from the measurements.

This section presents simulated scalar field reconstructions from point measurements and a tomography experiment. The example scalar field, shown in Figure 7, is randomly synthesized by the method of quasi-wavelets (QWs) (Goedecke et al., 2004; Wilson et al., 2004). The QWs have a continuous size distribution from 5 m to 25 m. For eddy sizes between these values, the synthesized QW field posseses a $k^{-5/3}$ Kolmogorov inertial subrange. The standard deviation of the scalar field was set to 0.3 $m\,s^{-1}$. The synthesized field has a spectrum close to von Kármán's although the lack of eddies smaller than about 5 m creates a high-wavenumber roll-off similar to a dissipative subrange. For the tomography simulations,

the travel time of rays between each source-receiver pair was determined through a numerical integration process. Random noise with a standard deviation of 10^{-5} s was added to the travel times to account for measurement errors.

To illustrate the outcome of using a length scale for the presumed correlation function that is too small, the stochastic inverses for the point measurements and tomography experiment were calculated with a Gaussian correlation function and ℓ_G = 10 m.[3] The resulting reconstructions are shown in Figures 8 and 9. The ability of the point measurements to find eddies is a "hit-or-miss" process. For example, two "hot spots" (high sound-speed) regions centered at approximately $(20, 10)$ and $(30, 30)$ are captured because sensors are present at these locations; a similar hot spot at $(30, 85)$ is largely missed because it was not close enough to any sensors. The tomography, being based on path-average measurements, provides a smoothed picture of the flow that does not miss substantial eddy activity. The domain-average, normalized mean-square error (i.e., $\mathrm{mean}\,[\mathrm{diag}\,(\mathbf{R}_{ee})]/\sigma^2$) was 0.54 for the point measurements and 0.29 for the tomography.

Figure 10 shows a tomographic reconstruction of the scalar field based on application of the generalized inverse method (Aki and Richards, 1980). This method uses a singular-value decomposition of the forward-problem solution and does not involve any *explicit* assumptions regarding the spatial statistical structure of the medium. For this example, the domain was partitioned into 25 grid cells, as shown in Figure 1. Since 81 data are being used to construct 25 models, the problem is overdetermined. Some correspondance between the generalized inverse results and the low and high sound-speed regions in the original data (Figure 7) are evident. However, the domain-average, normalized mean-square error was 1.1. That is, the tomography and generalized inverse method actually led to fields that were statistically less reliable than assuming the perturbations were zero. This outcome illustrates the undesirability of forcing a discontinuous inverse solution onto a continuous medium.

5. APPLICATION TO FLOW-IMAGING TOMOGRAPHY

The travel time of acoustic pulses in the atmosphere depends on the wind velocity as well as the sound speed. Because the effective speed of a ray is the actual sound speed plus the wind component in the propagation direction (this statement neglects refraction effects), ray paths at multiple angles through a given region allow both the sound speed and wind velocity to be determined. In this section, we simulate a tomography experiment where the sound-speed and wind-velocity fields are simultaneously

reconstructed. The sound-speed and wind-velocity fields were both randomly synthesized in the tomographic plane from QWs with sizes ranging from 5 m to 25 m. The sound speed and wind fields are synthesized separately and therefore are uncorrelated. The stochastic inverse was estimated based on a presumed Gaussian correlation function with ℓ_G = 10 m. The standard deviation was 0.3 m s^{-1} for the sound speed and 0.6 m s^{-1} for each of the wind components.

Figures 11–14 show the synthesized random wind fields and reconstructions. The domain-average, normalized mean-square error was 0.80 for the tomographic sound-speed reconstruction (not shown), 0.64 for the wind component in the *x*-direction, and 0.41 for the wind component in the *y*-direction. The error for the sound speed is highest because its contribution to the travel-time fluctuations is lowest in this example, and therefore the data contain the least information on that variable. The greater accuracy for the *y*-wind component relative to the *x* component was observed in this and several other random trials. It likely results from the ray paths being oriented more often along the *y*-direction than the *x*-direction. Arrays with ray paths having a more isotropic distribution in azimuth could avoid this effect.

6. CONCLUSION

Example simulations presented in this paper suggest that tomographic measurements can provide accurate, multi-dimensional images of atmospheric wind and temperature fields. In comparison to in-situ point sensors, the tomographic observations provide smoothly filtered fields that capture all strong activity in the measurement region. The smoothing effect of tomography could make it a useful alternative to point sensors for evaluating LES subfilter scale models (Sullivan et al., 2003). The "multiplier" effect of tomography (in which the number of observations grows as the product of the number of sources and receivers, rather than in proportion to the number of sensors) is also a valuable benefit. The challenge remains, however, of developing reliable, inexpensive, and reasonably easy-to-use hardware that performs acoustic tomography.

A particular problem studied in this paper was the effect on stochastic inverse calculations of mismatch between the presumed spatial correlation function for the atmospheric fields and the actual one. The results showed that an accurate inverse reconstructions can be obtained even when the presumed correlation function differs substantially from the actual one. In particular, near-optimal results can be obtained when the presumed outer length scale is approximately equal to or larger than the actual outer scale. Poor reconstructions occur when the presumed outer length scale is smaller than the actual one. In that case, the stochastic inverse method assumes no information of the fields far from the well probed part of the medium, and therefore sets the field perturbations to zero. Results also suggested that a Gaussian correlation function produces less satisfactory results than the
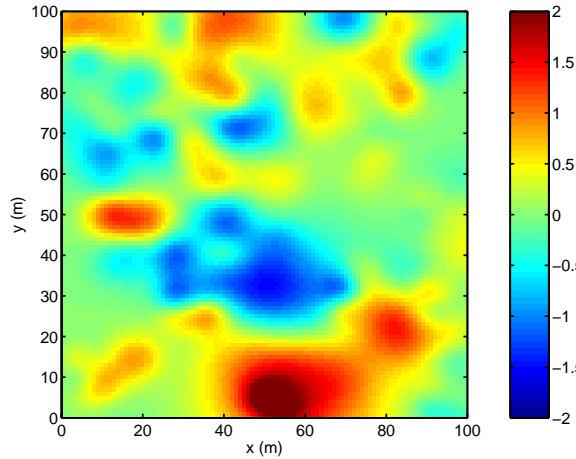
---

[3]All stochastic inverse reconstructions in this paper were performed on a grid of 101×101 grid points, yielding a 1-m resolution. This resolution was chosen because it produced visually smooth fields and carried a reasonable computational burden. Since the stochastic inverse estimate at a given model point is independent of all others, in principle the reconstruction can be done at an arbitrarily high resolution.

FIG. 11: Turbulent velocity field randomly synthesized by the QW method. The wind component in the *x*-direction is shown. Color scale is the wind speed in $\mathrm{m\,s^{-1}}$.
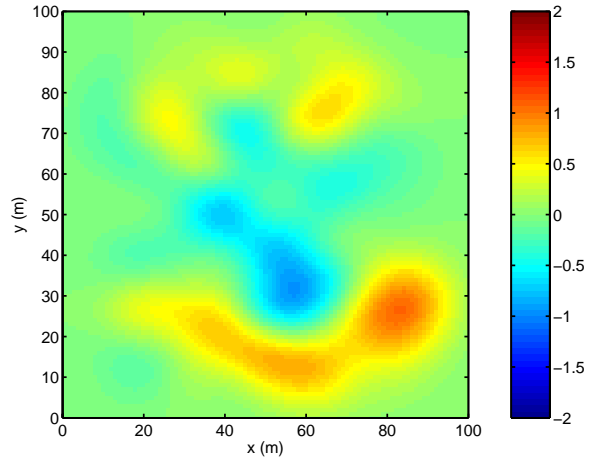

FIG. 13: Tomographic reconstruction of the wind component in the *x*-direction based on ray traces through the fields shown in Figures 11 and 12.
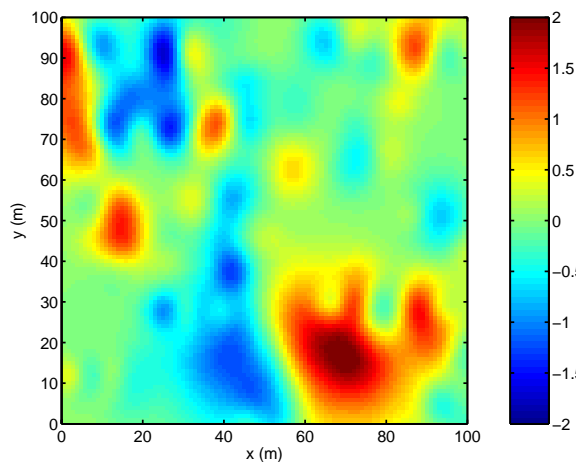

FIG. 12: Turbulent velocity field randomly synthesized by the QW method. The wind component in the *y*-direction is shown.
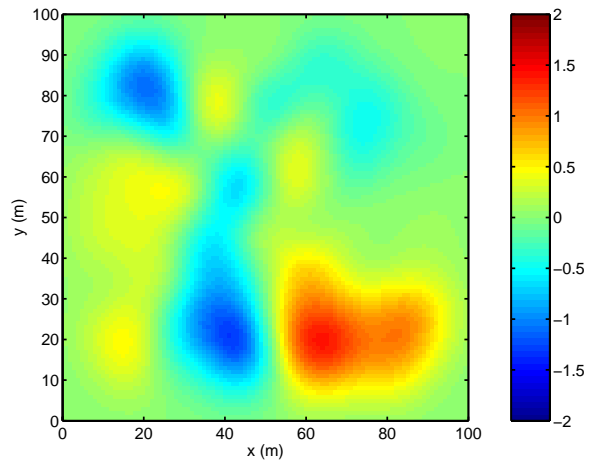

FIG. 14: Tomographic reconstruction of the wind component in the *y*-direction based on ray traces through the fields shown in Figures 11 and 12.

von Kármán and exponential correlation functions, particularly if the field is estimated at a point outside the densely probed part of the medium.

REFERENCES

Aki, K. and P. G. Richards, 1980: *Quantitative Seismology.* W. H. Freeman, New York.

Goedecke, G., V. E. Ostashev, D. K. Wilson, and H. J. Auvermann, 2004: Quasi-wavelet model of von Kármán spectrum of turbulent velocity fluctuations. *Boundary-Layer Meteorol.*, **112**, 33–56.

Sullivan, P. P., T. Horst, D. H. Lenschow, C.-H. Moeng, and J. C.

Weil, 2003: Structure of subfilter-scale fluxes in the atmospheric surface layer with application to les modeling. *J. Fluid Mech.*, **482**, 101–139.

Wilson, D. K., V. E. Ostashev, G. H. Goedecke, and H. J. Auvermann, 2004: Quasi-wavelet calculations of sound scattering behind barriers. *Appl. Acoust.*, **65**, 605–627.

Wilson, D. K. and D. W. Thomson, 1994: Acoustic tomographic monitoring of the atmospheric surface layer. *J. Atmos. Ocean. Tech.*, **11**, 751–769.

Wilson, D. K., A. Ziemann, V. E. Ostashev, and A. G. Voronovich, 2001: An overview of acoustic travel-time tomography in the atmosphere and its potential applications. *Acustica*, **87**, 721–730.

Ziemann, A., K. Arnold, and A. Raabe, 1999: Acoustic tomography in the atmospheric surface layer. *Ann. Geophys. - Atm. Hydr.*, **17**, 139–148.